Molecular Dynamics Simulations of Ordering of Poly(dimethylsiloxane) under Uniaxial Stress†

Naida M. Lacevic, Robert S. Maxwell, Andrew Saab, and Richard H. Gee*

Lawrence Livermore National Laboratory, Chemistry and Materials Science Directorate, University of California, Livermore, California 94551

Received: August 26, 2005; In Final Form: October 21, 2005

Molecular dynamics simulations of bulk melts of poly(dimethylsiloxane) (PDMS) are utilized to study chain conformation and ordering under constant stress uniaxial extension at room temperature. We find that large extensions induce chain ordering in the direction of applied stress. During the extension, we also find that voids are created via a cavitation mechanism. At the end of our simulations, by visual inspection, we distinguish cavity, fibril, and amorphous regions that coexist together. The surrounding material about the formed cavities is fibril-like, while the remaining material remains amorphous. We also estimate the surface energy of the cavity. The cavity size continually increases in the dimension of applied stress but saturates in the lateral dimensions, most likely due to the finite size of the system. Despite chain orientation and ordering in the direction of applied stress, crystallization is absent in the time and stress range of our simulation. This study represents a baseline for the future study of mechanical properties of PDMS melts enriched with fillers under stress.

I. Introduction

Poly(dimethysiloxane) (PDMS) is one of the most common silicones used for industrial purposes. PDMS has a wide range of applications such as adhesives, coatings, contact lenses, biomedical devices, lubricating oils, and heat resistant tiles among many others.[1−3] One of the most valuable features of PDMS is its ability to dramatically change its mechanical properties with the addition of inert filler particles to the pure PDMS system. A succinct account of some of the interesting features of PDMS can be found in refs 4 and 5.

The necessity to understand the deformation and reinforcing mechanisms that control PDMS/filler properties has motivated researchers to investigate, at the molecular level, the changes in structural and dynamical properties influenced by the filler (see, e.g., Gee et al.[6]). Molecular dynamics (MD) simulations provide an excellent tool to directly study the influence of the filler on material properties upon deformation, since the contact area between the filler and PDMS is difficult to characterize in experiment. These simulations can be very expensive if an explicit atom model is used. However, united-atom models allow for larger time steps and, therefore, longer and larger simulations. A recently developed hybrid united-atom model of PDMS by Frischknecht and Curro[7] is a great improvement over previous united-atom models of PDMS[8] because it uses stronger interactions between silicon (Si) and oxygen (O) atoms. The strength of this intermolecular interaction is very important because it increases PDMS thermal stability.[4] This model also gives reasonably good results in predicting the structural attributes of PDMS melts and is in good agreement with the explicit atom model of Sun et al.[9] All simulations presented in this work are performed using the hybrid PDMS model.

There have been numerous studies of polymer deformation under constant stress or strain using molecular dynamics techniques. Some of these works can be found in refs 10−14. The common feature in all MD simulations of extension is that the deformation rate is much higher than deformation rates that are typically used in experiments; it is conceivable that those rates could be achieved using laser ablation techniques[15] (assuming that complications such as bond breaking could be eliminated). Such extremely high deformation rates inevitably lead to mechanical failure of the material that is typically observed as a rupture. Material rupture is influenced by several factors such as stress relief via viscoelastic relaxation, crystallization at large extensions, and the presence of filler particles.[16−18] The purpose of this work is to obtain physical insight into pure PDMS melt behavior upon extension. The findings obtained from this study will help rationalize future investigations of silica filled PDMS systems under uniaxial extension.

The paper is organized as follows. In section II, we describe the model and methods used to produce our result. Section III is divided into three subsections. The first subsection deals with PDMS extension under various stresses and PDMS chain conformation. The second subsection deals with analysis of cavities and the corresponding surface energy. The third subsection deals with chain ordering and calculation of the orientational order parameters. We conclude with a discussion of our results in section IV.

II. Computational Methods

II.1. PDMS Melt Representation and Force Fields. Poly(dimethylsiloxane) is a macromolecule composed of repeating silicon−oxygen bonds along the backbone.[19] The chemical structure of the PDMS molecule is $[-O-Si(CH_3)_2-]_n$, where n is the number of repeat units or monomers. The united-atom model representation treats each carbon and its bonded hydrogen atoms as a single united particle, whereas Si and O atoms are each represented as individual particles. An extensive study of the structural and dynamical properties of the PDMS united-atom model used in this paper is described in ref 7. The force field is described by the following interactions: The bond, angle, and torsional potentials are represented by class I intermolecular

† Part of the special issue "Michael L. Klein Festschrift".

* Corresponding author. E-mail: gee10@llnl.gov.

10.1021/jp054845e CCC: $33.50
Published on Web 12/02/2005

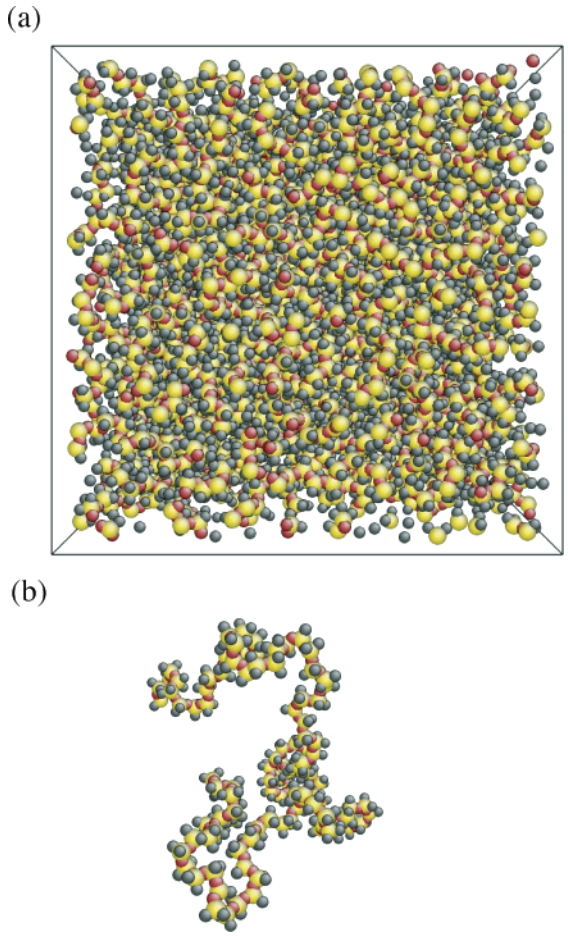

Figure 1. (a) Snapshot of the initial configuration of the PDMS melt before stress has been applied. The initial periodic simulation cell dimensions are 8.5 × 8.5 × 8.5 nm^3. (b) A single chain isolated from the melt. Red spheres represent oxygen (O) atoms, yellow spheres represent silicon (Si) atoms, and gray spheres represent united CH_3 "atoms".

potentials. The bond stretching and angle bending potentials are given by the usual harmonic potentials

$$E_{\text{bond}} = k_{\text{bond}}(r - l_0)^2 \tag{1}$$

and

$$E_{\text{angle}} = k_\theta(\theta - \theta_0)^2 \tag{2}$$

where the bond length and angle vary around an equilibrium value, l_0 and θ_0, respectively. The torsional potential is given by

$$E_{\text{torsion}} = k_t[1 + \cos(n\phi)] \tag{3}$$

The nonbonded interactions are van der Waals ($E^{\text{vw}}(r)$) and Coulomb potentials given by

$$E_{\text{nonbond}} = \begin{cases} E^{\text{vW}}_{\alpha\beta}(r) + k_q\dfrac{q_\alpha q_\beta}{r} & r < r_c \\ k_q\dfrac{q_\alpha q_\beta}{r} & r > r_c \end{cases} \tag{4}$$

where q is the charge, r is the distance between the two atoms α and β, r_c is the cutoff distance for the van der Waals interactions, and $k_q = 1/(4\pi\epsilon_0)$ (ϵ_0 is the dielectric constant). The difference between this model and models used in the past[8] is the intermolecular interaction between Si−Si, O−O, and Si−O atoms, $E^{\text{vW}}_{\alpha\beta}(r) = \epsilon_{\alpha\beta}[2(\sigma_{\alpha\beta}/r)^9 - 3(\sigma_{\alpha\beta}/r)^6]$, and for the intermolecular interaction between CH_3 groups, O−CH_3, and Si−CH_3, $E^{\text{vW}}_{\alpha\beta}(r) = 4\epsilon_{\alpha\beta}[(\sigma_{\alpha\beta}/r)^{12} - (\sigma_{\alpha\beta}/r)^6]$. The model is referred to as a "hybrid model" because of the "mixed" van der Waals interactions. The parameters for this model can be found in Table 1 of ref 7. The advantage of using this model is its more accurate representation of interactions on the backbone chain. The hybrid model has shown reasonable agreement with the results of an explicit atom model[9] for the intermolecular structure, pressure, and chain dimensions in the melt.[7]

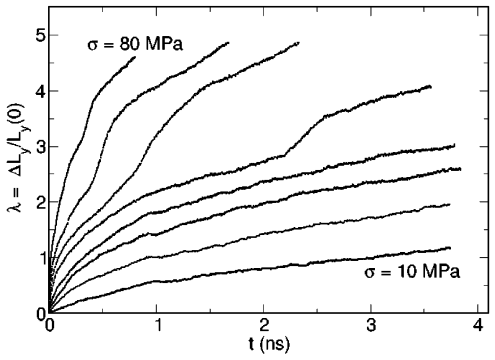

Figure 2. Strain, $\lambda(t) = \Delta L_y(t)/L_y(0)$, measured in the direction of applied stress as a function of time for each value of uniaxial stress (σ) in the range 10−80 MPa (in increments of 10 MPa). Stress values increase from the bottom up.

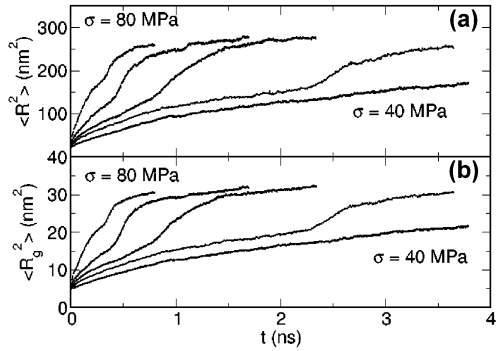

Figure 3. Mean square end-to-end distance ($\langle R^2\rangle$) (panel a) and mean square radius of gyration ($\langle R_g^2\rangle$) (panel b) for each value of uniaxial stress (σ) (40−80 MPa). Both $\langle R^2\rangle$ and $\langle R_g^2\rangle$ increase and reach a value that increases slowly compared to λ. Stress values increase from the bottom up.

Our simulations consisted of 40 120-mer PDMS polymer chains (19 200 total united-atoms), where each monomer contains a single Si and O atom, and two CH_3 united-atoms. The molecular weight of our PDMS chains is $M_w = 8880$ g/mol. The molecular weight between entanglements for PDMS is $M_e = 8100$ g/mol,[20] and since $M_c < M_w$, our melt is in the weakly entangled regime.

II.2. Molecular Dynamics Method. Here, we use MD to study the structural and dynamic changes in bulk PDMS melts under stress. This is a widely used method for the investigation of various physical processes related to the dynamics of materials (e.g., deformation of solids, polymer crystallization, aging in supercooled liquids, motion of biomolecules). MD provides static and dynamic properties for a collection of particles that allow atomic scale insights that are difficult to gain otherwise.

The amorphous PDMS polymer structures studied here were simulated using 3D cubic periodic boundary conditions. The initial configurations were generated using constant particle

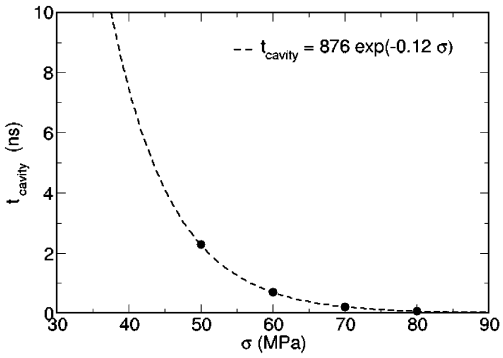

Figure 4. Stress dependence of the onset of cavitation (circles). The solid line is a fit to an exponential function. At lower stresses, the onset of cavitation appears at much longer times.

number, pressure, and temperature (*NPT*) dynamics at zero pressure. The velocity Verlet[21] time integration method was used with a time step of 1 fs. The Andersen[22] method was used for constant *NPT* dynamics. The initial PDMS configuration was generated such that the bulk density was 0.7 g/cm^3. The lower density initial state was found to improve the convergence of the equilibration procedure by avoiding high-energy initial configurations. The bulk PDMS ensemble was then simulated at 550 K, where the periodic box was allowed to relax under *NPT* conditions. The volume equilibration process was carried out for a minimum duration of 5 ns. Following this step, the system was cooled in *NPT* runs in increments of 50 K and equilibrated for 5 ns each at the incremental temperatures down to 300 K.

After the initial equilibration process, simulations were performed under constant stress (σ) at 300 K in $N\sigma T$ MD runs. The constant stress was applied uniaxially along the *y*-axis of the periodic simulation cell. The initial simulation cell is shown in Figure 1a. A single chain, isolated from the melt, is shown in Figure 1b. In all extension simulations, the applied constant stress ranged from 10 to 80 MPa. The normal stress on the other faces of the simulation box was set to zero. For the extension simulations, we used a standard Nose−Hoover thermostat and barostat.[23] The coupling constants for the barostat and thermostat are 1000 and 100 fs, respectively, and they are kept constant for all extension simulations. All computations were carried out with a modified version of LAMMPS.[24]

III. Results and Discussion

III.1. Constant Stress Deformation. Uniaxial deformation via constant stress along the *y*-axis of the periodic simulation cell is applied to a pure PDMS melt. Figure 2 shows strain (in the direction of applied stress), $\lambda(t) = \Delta L_y(t)/L_y(0)$, as a function of time for the stress range 10−80 MPa in increments of 10 MPa at 300 K, where $\Delta L_y(t) = L_y(t) - L_y(0)$ and $L_y(0)$ is the initial box length. The strain ($\lambda(t)$) increases and develops a shoulder at short times and then steadily increases at later times. Similar observations for strain were made in a recent simulation study of polyethylene (PE) melts under uniaxial extension by Lavine et al.[25] The authors investigated crystallization and ordering of PE chains during uniaxial extension and found that "the addition of a large deforming stress accelerates ordering and the crystallization process" which is a major motivation for our work. Note that, at later times, each strain curve in the stress range from 50 to 80 MPa exhibits a region where λ is almost linear in time, which means that the strain rate is constant during this interval, and after that, strain continues to increase.

To quantify the chains' structural properties during the extension, we calculated the mean square end-to-end distance ($\langle R^2 \rangle$) (shown in Figure 3a) and the mean square radius of gyration ($\langle R_g^2 \rangle$) (shown in Figure 3b). We find that these quantities increase in time at all stress values displaying an initial rise and shoulder (similar to λ) and increase at later times. We note that both $\langle R^2 \rangle$ and $\langle R_g^2 \rangle$ (for the stress range 50−80 MPa)

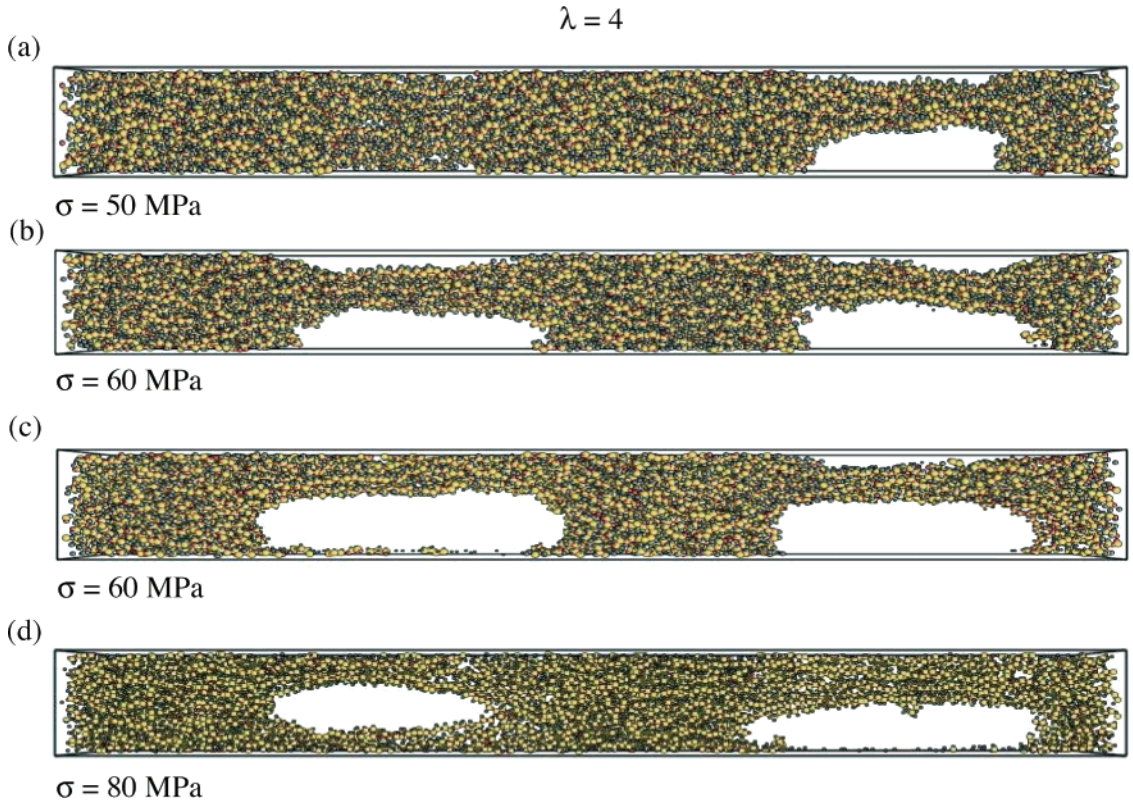

Figure 5. Snapshots of cavities at $\lambda = 4$ at long times for various stress values (σ). At higher stresses, material cavitates at two places.

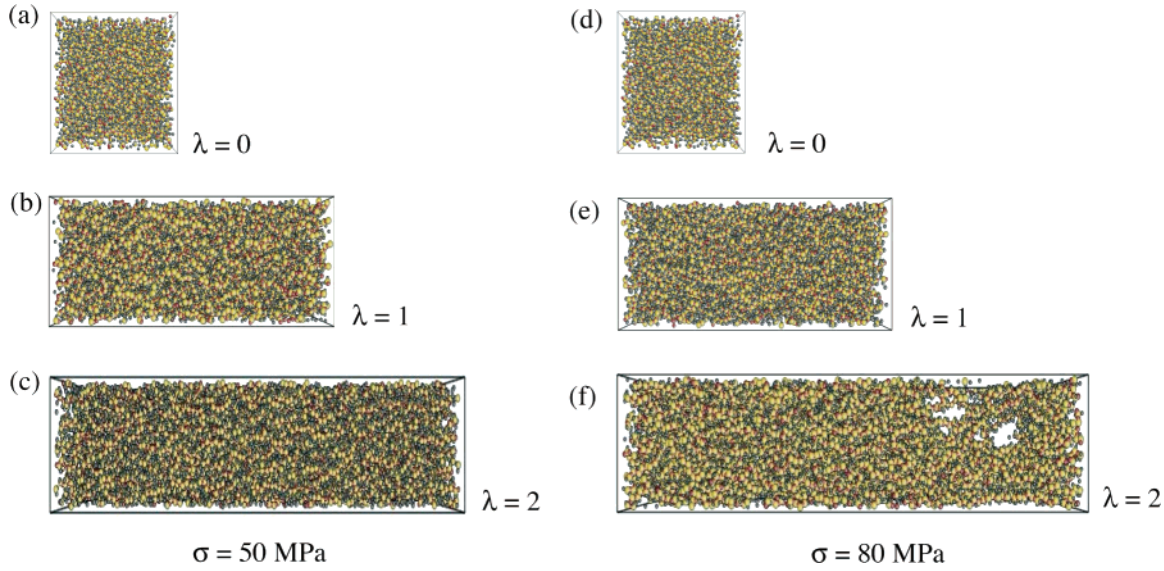

Figure 6. Snapshots of our simulations of PDMS under extension. The columns represent systems at strain values of $\lambda = 0$ (initial sample), $\lambda = 1$, and $\lambda = 2$, respectively. The applied stress is 50 MPa (a−c) and 80 MPa (d−f). We observe that the sample cavitates at long times and high values of uniaxial stress.

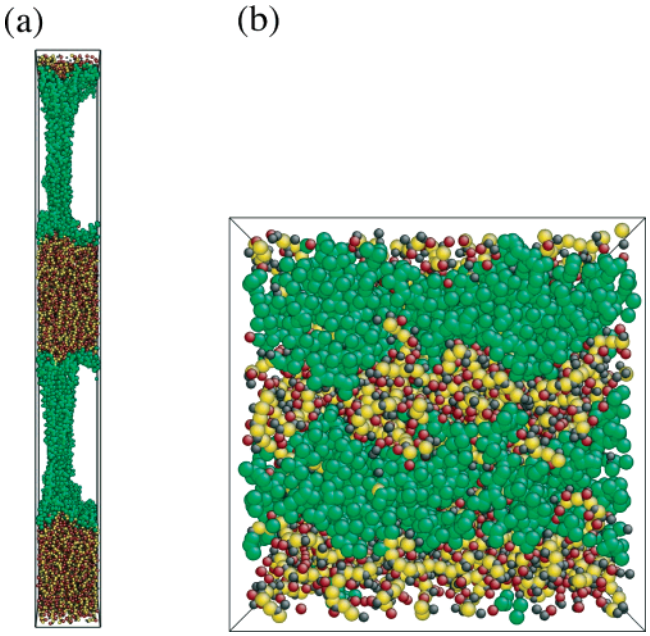

Figure 7. (a) Snapshot of the PMDS melt at $\sigma = 60$ MPa and $t = 1.5$ ns. Particles that are on the surface of the cavity are shown in green. (b) The initial configuration of the PDMS melt and cavity particles is traced back to the initial configuration and shown in green.

increase at a similar rate after the shoulder, which may be affected by the finite size of our system.

III.2. Cavitation. Visual inspection of the PDMS melt configurations at various times indicates that voids form at certain times (or certain points on the strain curve in Figure 2) for sufficiently high stresses. We find that the onset of the linear region in Figure 2 is correlated to the appearance of voids or cavities (see Figure 6f). From this time dependent behavior of λ (Figure 2), it is possible to estimate the range of stress for which the PDMS melt can support the stress for the duration of our simulations. To determine this range, we select PDMS configurations just before λ enters the linear region. This is only possible for the stress values from 50 to 80 MPa because λ at lower stress does not exhibit such behavior. Figure 4 shows the time at which each PDMS melt starts to cavitate (or λ becomes linear in time) versus applied stress. We are able to fit t_{cavity} to an exponential function of applied stress. From this functional form, it is possible to extrapolate times at which a PDMS melt would cavitate at lower stress (e.g., for $\sigma = 40$ MPa, it would take approximately 8 ns to observe cavitation). In this manner, we are able to estimate the range of stress which a PDMS melt can support without cavitation. Such information will be useful for future studies of filler/melt systems.

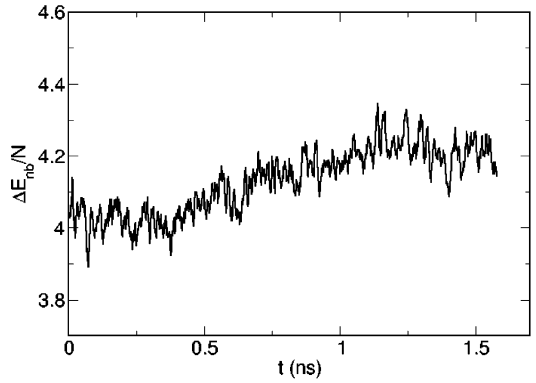

Figure 8. Time dependence of the difference between nonbonded energy per particle of the total system and nonbonded energy per particle of the cavity at $\sigma = 60$ MPa.

Cavity formation can be considered as an energy balance between the strain energy relieved by cavitation and the surface energy associated with the generation of the new surfaces.[26] Figure 5 shows cavities at strain $\lambda = 4$ for stresses in the range from 50 to 80 MPa in our simulations. We note that the volume of the cavities increases as the stress increases. The structure observed at high strain for all stresses is similar to a crazing structure for which the microscopic origin is explained in great detail by Kramer.[27] The idea is that the absence of entanglement of chains is important for fibril formation. The relatively small system and very fast deformation rate will yield a small craze dimension, and we do not attempt to estimate it here. We note that crazing typically occurs in linear polymer glasses.[28,29] Our simulations are performed at room temperature, which is well above the glass transition temperature of PDMS under ambient conditions; however, due to the extremely high strain rates imposed in our simulations, the PDMS polymers are unable to

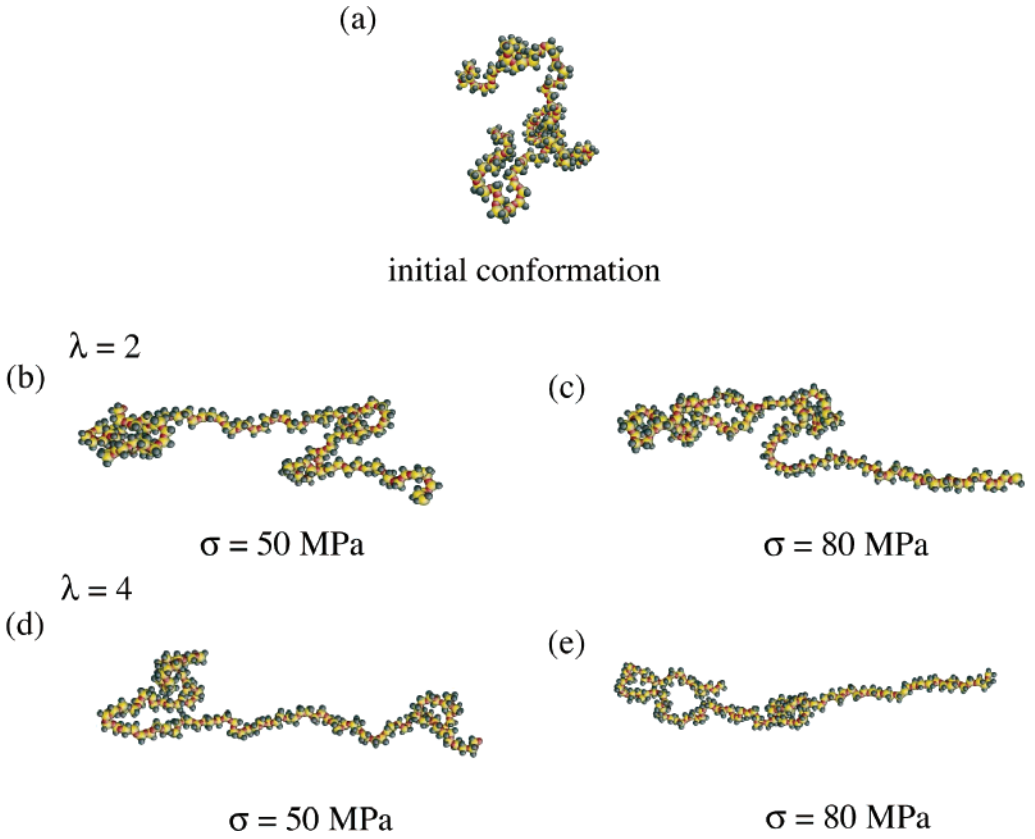

Figure 9. Single chain conformations at $\lambda = 0$ (initial configuration) (a) and (b and c) for $\lambda = 2$ and (d and e) for $\lambda = 4$ at $\sigma = 50$ MPa and $\sigma = 80$ MPa, respectively.

fully relax; thus, the PDMS polymer chains are effectively glassy, where the occurrence of crazing is consistent (as seen both experimentally[28] and from simulations[30]).

We inspect several PDMS configurations at low and high stress values and identify the monomers that belong to the surface of the cavities. At low stress, the material can support extension up to nearly $\lambda = 3$ before it starts to cavitate. At higher stress, the material can only support extension up to $\lambda = 1.5$. Figure 6 shows "snapshots" of our simulated system at strains of $\lambda = 0$, 1.0, and 2 for a relatively low uniaxial stress, $\sigma = 50$ MPa (Figure 6a−c), and a higher stress, $\sigma = 80$ MPa (Figure 6d−f). We observe three regions in the PDMS melt at later times during our simulations: amorphous, cavity, and fibrils. Fiber regions always appear closer to cavities. This is not surprising because chains need to extend (elongate) to provide space for a cavity. These observations are consistent with earlier experimental[31] and simulation[13,27,32,33] studies of deformation in other polymers.

One of the obvious questions suggested by the observation of cavitation is the following: what is the energy cost of cavity formation or surface energy? There are several methods of determining the surface energy of the cavity. The most obvious method is to determine the cohesive energy of the system at the same state point with and without a cavity. The cohesive energy in our case is the energy of the system due to nonbonded interactions (i.e., Coulomb and van der Waals energy contributions). However, after the system reaches a strain at which cavitation occurs, it is not possible to relax the system at that strain so that cavity disappears.

Another method for estimating the surface energy of the cavity is to identify monomers on the surface of the cavity and calculate their nonbonded energy. We select the monomers that are close to the surface of the cavity by visual inspection, as shown in Figure 7a. Figure 7b shows the initial positions of particles that make up the surface of the cavity at late time, $\lambda = 4$ under $\sigma = 60$ MPa. The particles that belong to the cavity surface form lamella-like structures (green regions in Figure 7b), and these lamellae are perpendicular to the axes of extension at the initial time. This demonstrates that cavitation is a highly localized process because the lamellae remain preserved until cavity formation. Furthermore, monomers forming the cavity surface do not move very much during the void formation. We follow cavity monomers in time and calculate their nonbonded energy. Figure 8 shows the time dependence of the difference in the nonbonded energy ($\Delta E_{nb}(t)$) between the monomers that do not belong to the cavity (E^{tot}_{nb}) and the monomers on the surface of the cavity (E^{cavity}_{nb}).

To estimate the surface energy of the cavity, we calculate the average number of monomers per surface area and multiply this number by the energy difference (ΔE_{nb}) at a given time. The density of our system is $\rho = 0.7$ g/cm^3 (the number density is 22.8 nm^{-3}); therefore, a rough estimate of the average number of monomers on the surface is $N_{surface} = \sqrt[2/3]{\rho} = 8.03$ nm^{-2}. At $\lambda = 4$ and $\sigma = 60$ MPa, the surface energy of the monomer in the cavity is $\gamma = \Delta E_{nb} N_{surface} = 230$ mJ/m^2. This value is larger than the one obtained in experiments[34] which ranges from 10 to 100 mJ/m^2, possibly because of the relatively low density of our system.

III.3. Melt Ordering. Since crystallization of PE has been observed in ref 25 due to ordering resulting from extension, the question of whether the same effect would be noted here arises. It is apparent that ordering and changes in chain conformation occur during our PDMS extension, and we quantify this here. Figure 9 shows a single PDMS chain isolated from the melt, at its initial configuration (Figure 9a) and $\lambda = 2$ at $\sigma = 50$ MPa (Figure 9b) and $\sigma = 80$ MPa (Figure 9c) and λ

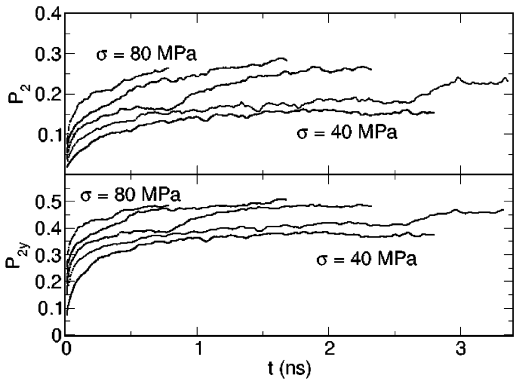

Figure 10. Time dependence of the orientational parameters P_2 and P_{2y} at various stresses. Both P_2 and P_{2y} are increasing in time. Stress values increase from the bottom up.

$= 4$ at $\sigma = 50$ MPa (Figure 9d) and $\sigma = 80$ MPa (Figure 9e), respectively. We observe that the chain at $\sigma = 80$ MPa is more elongated compared to the chain at $\sigma = 50$ MPa at the same strain value.

The chain dynamics for are PDMS systems upon extension are monitored by the evolution of the global orientational order parameters:

$$P_2 = \left\langle \frac{3\cos^2\theta - 1}{2} \right\rangle \quad (1)$$

where θ is the angle between two "chord" vectors and $\langle ... \rangle$ denotes the average over all chord pairs, and

$$P_{2y} = \left\langle \frac{3\cos^2\theta_y - 1}{2} \right\rangle \quad (2)$$

where θ_y is the angle between the chord vector and the direction in which the stress is applied. A chord is defined as a line segment connecting two second nearest neighbors on the same chain. The angle (θ) is the dot product between every other chord vector defined in this way.

Figure 10 shows the time and stress dependence of P_2 and P_{2y}. P_2 and P_{2y} are calculated between every other chord vector. Both P_2 and P_{2y} increase in magnitude as the stress increases, confirming previous observations that the backbones of the polymer chains are rapidly aligned under uniaxial extension.[25] In previous studies of simpler polymers, this results in crystallization.[25] The alignment of the backbone of the chain may be a necessary condition for crystallization, but in the case of PDMS, it is apparently not sufficient. We do not observe crystallization of PMDS on the time scales studied. It is possible that the mechanisms for crystallization for PDMS melts are different from those of simpler polymers such as PE studied in ref 25, due to the presence of the two CH_3 groups whose alignment is an important factor for crystallization.

Figure 11 shows the time dependence of P_2 and P_{2y} for the monomers which will form the surface of the cavity at late times. At the initial time, the monomers are randomly oriented with respect to the direction of extension, reflected in the near zero values of P_{2y}. At later times, P_{2y} increases to a larger value than P_2, which is a manifestation of the onset of fibril formation about the cavity. This may have a significant effect on the filled PDMS system, since the chains may also align on the surfaces of the filler particles. Thus, functionalizing the filler to modify the interfacial energy and improve adhesion with PDMS may prove to be important. Future work will include simulations of filled PDMS melts under tension, where different functionalized surfaces will be investigated.

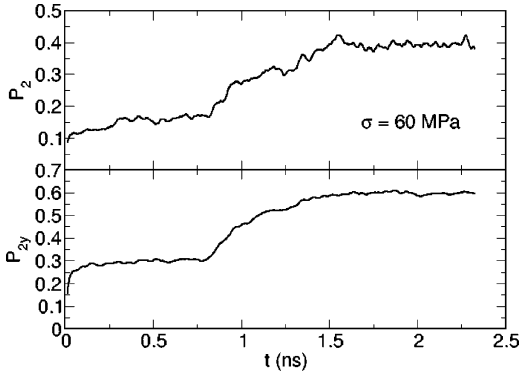

Figure 11. Time dependence of the orientational parameters P_2 and P_{2y} at $\sigma = 60$ MPa for the monomers on the surface of the cavity. P_2 and P_{2y} show a significant increase in ordering as compared to their bulk counterparts.

IV. Conclusions

In this paper, we present a study of PDMS melt properties upon uniaxial extension. We show that chains become elongated and ordered as a function of applied stress and time. We also find that the PDMS melt cavitates at high stress. The cavity formation is directly related to the mechanical properties of the material; therefore, addition of filler should effect the material deformation. We calculated the surface energy of the cavity and the orientational order parameter for the monomers on the surface of the cavity. Monomer alignment on the surface of the cavity may have significant effects on the PDMS melt/filler system. Further, we observe changes in the conformation of the polymer backbone as are seen in polyethylene, but we do not observe crystallization, possibly due to the pendent CH_3 groups which disrupt the overall order upon extension.

Acknowledgment. The work was performed under the auspices of the U.S. Department of Energy by the University of California Lawrence Livermore National Laboratory under contract W-7405-Eng-48. We thank Amitesh Maiti for useful discussion and the Livermore Computing for generous amounts of CPU time on Thunder and MCR clusters.

References and Notes

(1) Zeigher, J. M.; Fearon, F. W. G. *Silicon Based Polymer Science: A Comprehensive Resource*; ACS Press: Washington, DC, 1990; Vol. 224.
(2) Kraus, G. *Rubber Chem. Technol*. **1965**, *38*, 1070.
(3) Vondracek, A. P. *Rubber Chem. Technol.* **1990**, *63*, 220.
(4) Mark, J. E. *Acc. Chem. Res.* **2004**, *37*, 946.
(5) Mark, J. E. *Prog. Polym. Sci.* **2003**, *28*, 1205.
(6) Gee, R. H.; Maxwell, R. S.; Balazs, B. *Polymer* **2004**, *45*, 3885.
(7) Frischknecht, A. L.; Curro, J. G. *Macromolecules* **2003**, *36*, 2122.
(8) Sides, S. W.; Curro, J.; Grest, G. S.; Stevens, M. J.; Soddemann, T.; Habenschuss, A.; Londono, J. D. *Macromolecules* **2002**, *35*, 6455.
(9) Sun, H.; Rigby, D. *Spectrochim. Acta, Part A* **1997**, *53*, 1301.
(10) Brown, D.; Clarke, J. H. R. *Macromolecules* **1991**, *24*, 2075.
(11) Andoh, H.; Yamamoto, T. *Kobunshi Ronbunshu* **1996**, *53*, 660.
(12) Gestoso, P.; Brisson, J. *J. Polym. Sci., Part B: Polym. Phys.* **2002**, *40*, 1601.
(13) Ogura, I.; Yamamoto, T. *Polymer* **1995**, *36*, 1375.
(14) Xu, P.; Mark, J. E. *Makromol. Chem., Macromol. Chem. Phys.* **1991**, *192*, 567.
(15) Hare, D. E.; Dlott, D. D. *Appl. Phys. Lett.* **1994**, *64*, 715.
(16) Ferry, J. D. *Viscoelastic properties of polymers*, 3rd ed.; John Wiley & Sons: New York, 1980.
(17) *Science and Technology of Rubber*; Eirich, F. R., Ed.; Academic Press: 1978.
(18) Dannenberg, E. M. *Rubber Chem. Technol.* **1975**, *48*, 419.
(19) Voronkov, G. M.; Milileshevich, V. P.; Yuzhelevich, Y. A. 1978.

(20) Graessly, W. W. *Adv. Polym. Sci.* **1974**, *16*, 1.
(21) Allen, M. P.; Tildesley, D. J. *Computer Simulation of Liquids*; Clarendon Press: Oxford, U.K., 1989.
(22) Andersen, H. C. *J. Chem. Phys*. **1980**, *72*, 2384.
(23) Nose, S. *Mol. Phys.* **1984**, *52*, 255.
(24) Plimpton, S. J. *J. Comput. Phys.* **1995**, *117*, 1.
(25) Lavine, M. S.; Waheed, N.; Rutledge, G. C. *Polymer* **2003**, *44*, 1771.
(26) Dompas, D.; Groeninckx, G. *Polymer* **1994**, *35*, 4743.
(27) Kramer, E. J. *Adv. Polym. Sci.* **1983**, *52*−*53*, 1.
(28) Brown, H. R. *Macromolecules* **1991**, *24*, 2752.
(29) Rottler, J.; Robbins, M. O. *J. Adhes. Sci. Technol.* **2003**, *17*, 369.
(30) Rottler, J.; Robbins, M. O. *Comput. Phys. Commun.* **2005**, *169*, 177.
(31) Chinn, S.; DeTeresa, S.; Sawvel, A.; Shields, A.; Balazs, B.; Maxwell, R. S. *Polym. Degrad. Stab.*, in press.
(32) Stevens, M. J. *Macromolecules* **2001**, *34*, 2710.
(33) Baljon, A. R. C.; Robbins, M. O. *Macromolecules* **2001**, *34*, 4200.
(34) Castellano, M.; Conzatti, L.; Costa, G.; Falqui, L.; Turturro, A.; Valenti, B.; Negroni, F. *Polymer* **2005**, *46*, 695.